Supplemental Digital Content

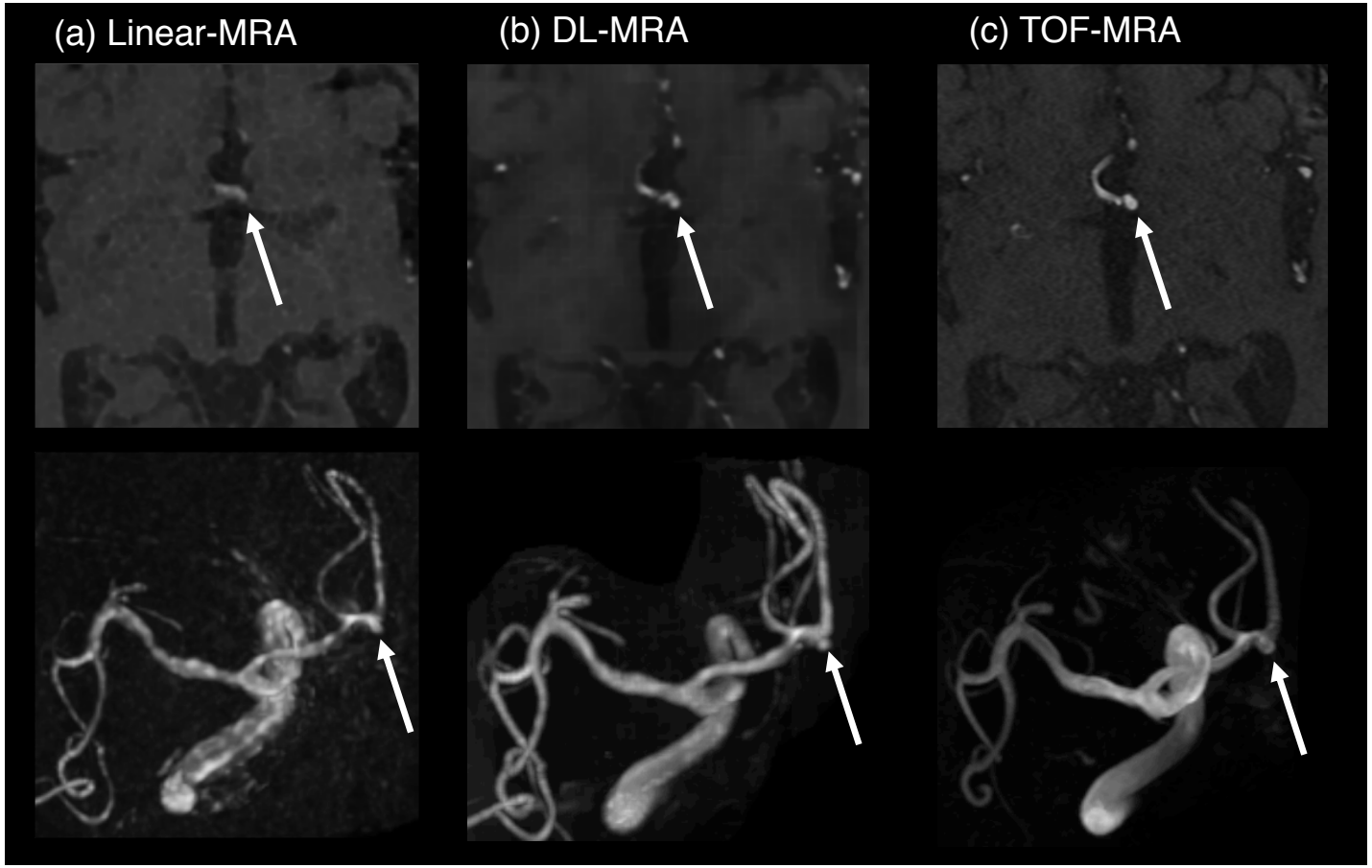

Supplementary Figure 1. A 76-year-old man with a left anterior cerebral artery aneurysm. Images based on the linear combination approach (a), DL approach (b), and TOF-MRA (c) are shown. White arrows show the aneurysm. The first row shows representative axial slices, and the second row shows the corresponding transverse maximum intensity projections. Note that the aneurysm looks smaller on (a) than (b) or (c). DL, deep learning; TOF, time-of-flight.

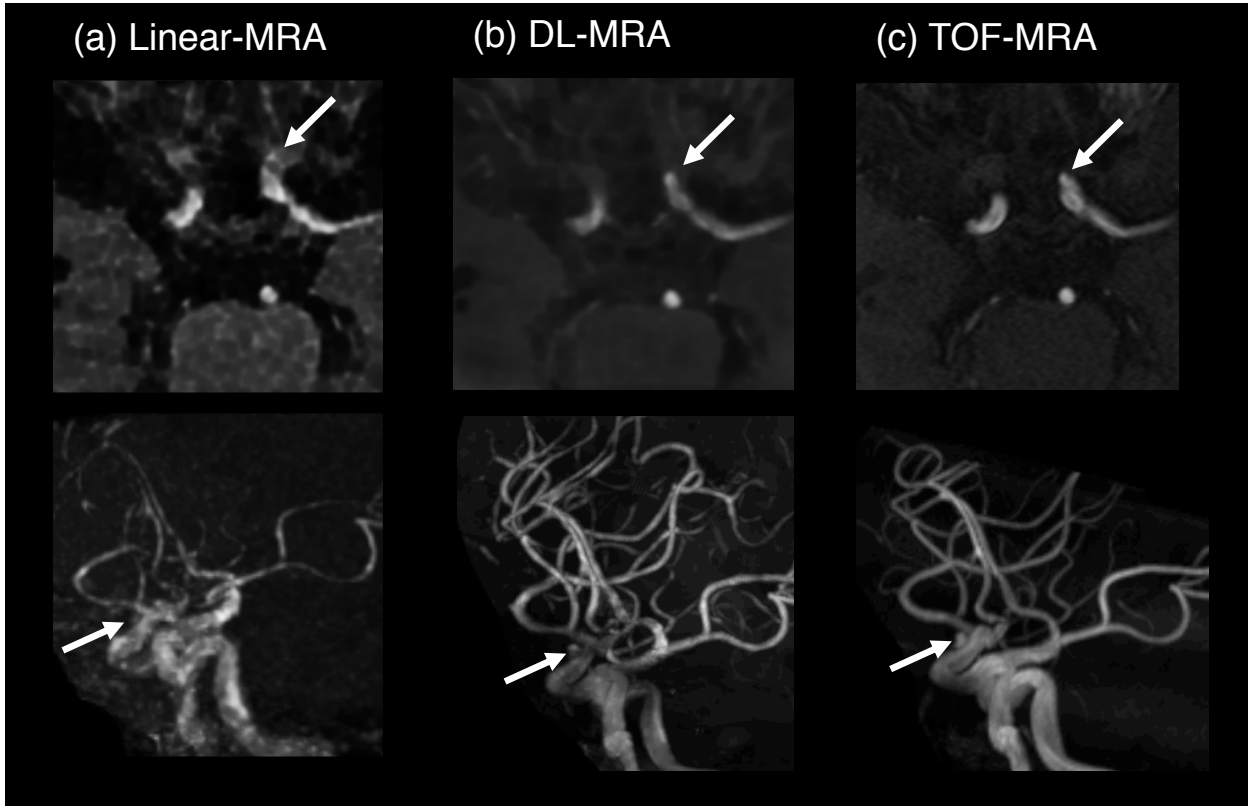

Supplementary Figure 2. A 75-year-old man with a left internal carotid artery aneurysm. Images based on the linear combination approach (a), DL approach (b), and TOF-MRA (c) are shown. White arrows show the aneurysm. The first row shows representative axial slices, and the second row shows the corresponding lateral maximum intensity projections. Note that the aneurysm is poorly demarcated on (a). DL, deep learning; TOF, time-of-flight.

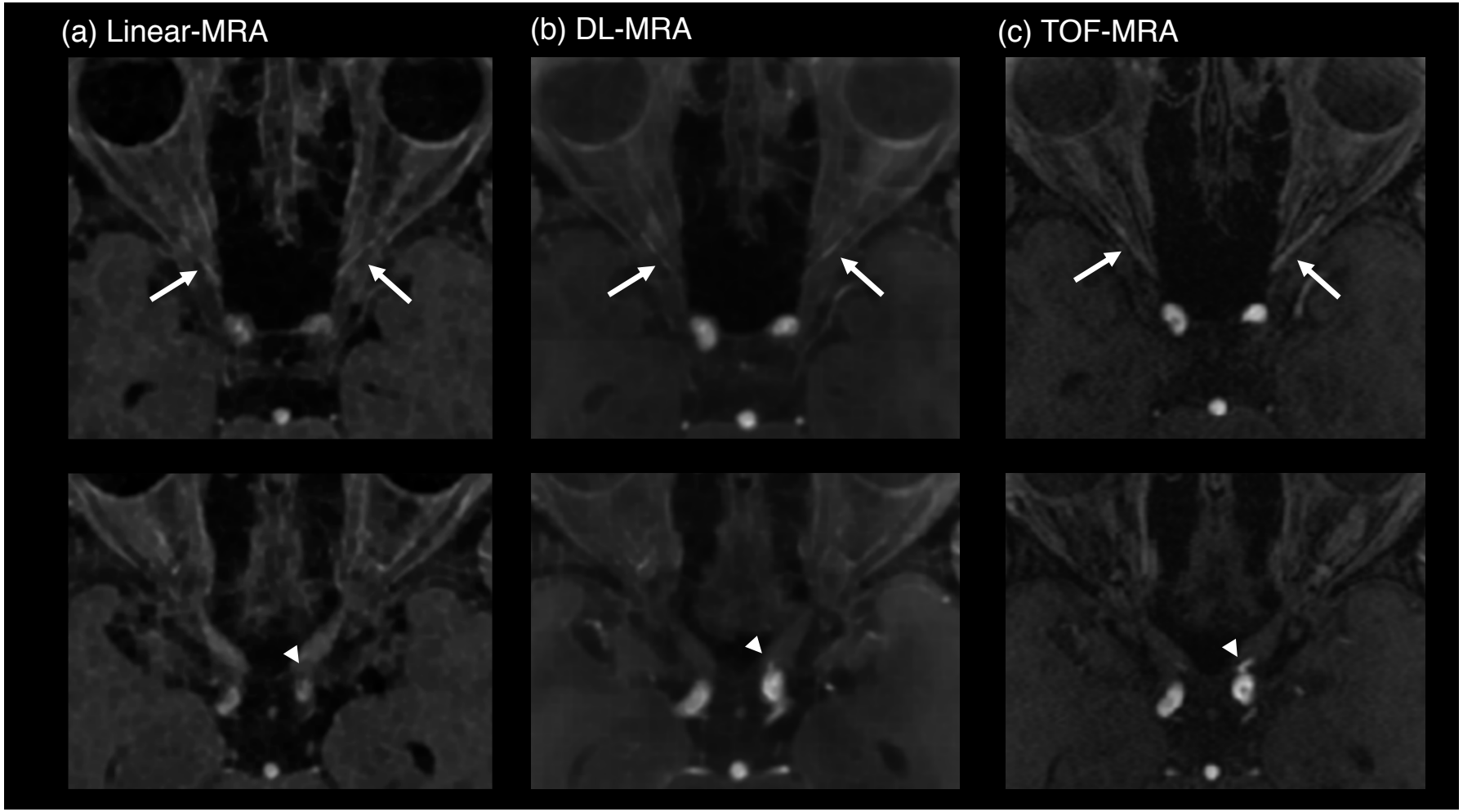

Supplementary Figure 3. Examples of ophthalmic artery visualization. Images based on the linear combination approach (a), DL approach (b), and TOF-MRA (c) are shown. The first row shows axial slices at the intra-orbital portion of the ophthalmic arteries (arrows), and the second row shows the corresponding axial slices at the origin of the left ophthalmic artery (arrowheads) from the internal carotid artery. Note that ophthalmic arteries are more poorly delineated on linear-MRA and DL-MRA than TOF-MRA. The visibility of these ophthalmic arteries was rated as 1, 2, and 4 by both neuroradiologists for the linear-MRA, DL-MRA, and TOF-MRA images, respectively. DL, deep learning; TOF, time-of-flight.